PHYSICAL REVIEW A **89**, 021802(R) (2014)

Double-double electromagnetically induced transparency with amplification

Hessa M. M. Alotaibi[1,2,*] and Barry C. Sanders[1,3]

[1]*Institute for Quantum Science and Technology, University of Calgary, Calgary, Alberta, Canada T2N 1N4*

[2]*Public Authority for Applied Education and Training, P.O. Box 23167, Safat 13092, Kuwait*

[3]*Hefei National Laboratory for Physical Sciences at Microscale, University of Science and Technology of China, Anhui 230026, China*

(Received 16 October 2013; published 27 February 2014)

We show that an alkali-metal atom with a tripod electronic structure can yield rich electromagnetically-induced-transparency phenomena even at room temperature. In particular we introduce double-double electromagnetically induced transparency wherein signal and probe fields each have two transparency windows. Their group velocities can be matched in either the first or second pair of transparency windows. Moreover, signal and probe fields can each experience coherent gain in the second transparency windows. We explain using a semiclassical dressed picture to connect the tripod electronic structure to a double-Λ scheme.

DOI: 10.1103/PhysRevA.89.021802 PACS number(s): 42.50.Gy, 42.50.Ex

Electromagnetically induced transparency (EIT) exploits interfering electronic transitions in a medium to eliminate absorption and dramatically modify dispersion over a narrow frequency band with applications including slow light, reduced self-focusing and defocusing [1], and quantum memory [2]. Microscopically, a three-level Λ electronic structure suffices to explain EIT. Double EIT (DEIT) extends EIT to creating two simultaneous transparency windows, one for a signal and the other for a probe field, with the aid of a third coupling field [3–7]. Double EIT is valuable for coherent control and enabling long-lived nonlinear interactions between weak fields, which could enable deterministic all-optical two-qubit gates for quantum computing.

Whereas the Λ atom suffices to explain EIT, DEIT requires at least four levels such as the tripod $\Lambda\!\!\Lambda$ atom [3] in Fig. 1(a). The same atom is shown in Fig. 1(b) for the semiclassical dressed state picture [8], which has two lower ($|1\rangle$ and $|3\rangle$) and two upper ($|\pm\rangle$) levels after eliminating the strong coupling (c) field. We introduce the semiclassical dressed representation of the $\Lambda\!\!\Lambda$-atom master equation as a powerful tool for intuiting double-DEIT phenomena including amplification.

This semiclassical dressed model of the $\Lambda\!\!\Lambda$ scheme corresponds effectively to a double Λ system, and double Λ schemes have been studied experimentally [9]. With our semiclassical dressed state analogy, we show that this $\Lambda\!\!\Lambda$ electronic structure exhibits rich EIT phenomena, namely, what we now call double-DEIT (DDEIT). Our DDEIT phenomenon has the property that both the signal and the probe fields can each have two EIT windows given the right parameter choices. The wide importance of EIT in, for example, slow light in atomic vapors [7], optical fibers [10], and Bose-Einstein condensates [11] as well as in solid-state systems such as optonanomechanics [12] and superconducting artificial atoms [13], indicates the broad applicability of our DDEIT properties.

One particular aspect of our system, namely, the second EIT window for the probe, has been predicted [14] and observed experimentally [7,15], but this previously observed effect corresponds only to one aspect of our system, namely, a double window for the probe and not to our full DDEIT for both signal and probe fields. Moreover, previous work on the $\Lambda\!\!\Lambda$-atom scheme focused on equal detuning between driving fields, whereas we are exploring rich phenomena outside this restrictive domain. These second EIT windows for each of the signal and probe fields exhibit coherent gain, which had not previously been expected. We now reprise the dynamics of the driven $\Lambda\!\!\Lambda$ atom [3]. For $\hbar \equiv 1$ and $\hat{\sigma}_{\iota\jmath} := |\iota\rangle\langle\jmath|$, the free Hamiltonian is $\hat{H}_0 = \sum_{\iota=1}^{4} \omega_\iota \sigma_{\iota\iota}$. For $\omega_{\iota\jmath} := \omega_\iota - \omega_\jmath$, the $\Lambda\!\!\Lambda$ atom is driven by a probe field with frequency $\omega_p = \omega_{41} - \delta_p$, a coupling field with frequency $\omega_c = \omega_{42} - \delta_c$, and a signal field with frequency $\omega_s = \omega_{43} - \delta_s$. In terms of Rabi frequencies Ω_x for $x \in \{p,c,s\}$, the driving Hamiltonian is $\hat{H}_{\rm dr}(t) = \frac{1}{2}(\Omega_p e^{i\omega_p t}\hat{\sigma}_{14} + \Omega_c e^{i\omega_c t}\hat{\sigma}_{24} + \Omega_s e^{i\omega_s t}\hat{\sigma}_{34} + \text{H.c.})$, with H.c. the Hermitian conjugate.

Under a rotating-frame transformation with respect to $\hat{A} = 3\delta_p\hat{\sigma}_{11} + (2\delta_p + \delta_c)\sigma_{22} + (2\delta_p + \delta_s)\hat{\sigma}_{33} + 2\delta_p\hat{\sigma}_{44}$, the resultant time-independent Hamiltonian is [3] $\hat{H} = \delta_{pc}\sigma_{22} + \delta_{ps}\sigma_{33} + \delta_p\sigma_{44} + (\Omega_p\sigma_{41} + \Omega_c\sigma_{42} + \Omega_s\sigma_{43} + \text{H.c.})/2$, with $\delta_{xy} := \delta_x - \delta_y$. The Lindblad master equation is

$$\dot{\rho} = i[\rho,\hat{H}] + \sum_{\iota<\jmath}^{4} \frac{\gamma_{\jmath\iota}}{2}(\sigma_{ij}\rho\sigma_{ji} - \sigma_{jj}\rho - \rho\sigma_{jj}) + \sum_{j=1}^{4} \frac{\gamma_{\phi j}}{2}(\sigma_{jj}\rho\sigma_{jj} - \sigma_{jj}\rho - \rho\sigma_{jj}), \quad (1)$$

including spontaneous emission and dephasing. The decay rates depicted in Fig. 1(a) are $\gamma_j := \sum_{i<j}(\gamma_{ji} + \gamma_{\phi j})$ and the steady-state density-matrix $\bar{\rho}$ solution is known [3]. We now provide analytic solutions, which we verified numerically by solving Eq. (1) in the steady state.

Given $\bar{\rho}$, optical susceptibility of the $\Lambda\!\!\Lambda$ medium can be calculated. We first consider the probe-field case and later the signal-field case, which is similar. We calculate the optical response to the probe field using the off-diagonal steady-state density-matrix element $\bar{\rho}_{14}$,

$$\bar{\rho}_{14} = \Omega_p \frac{i(\rho_{11} - \rho_{44}) + \frac{\Omega_s}{\gamma_3 - 2i\delta_{ps}}\bar{\rho}_{43}}{\gamma_4 - 2i\delta_p + \frac{|\Omega_c|^2}{\gamma_2 - 2i\delta_{pc}} + \frac{|\Omega_s|^2}{\gamma_3 - 2i\delta_{ps}}}, \quad (2)$$

with

$$\bar{\rho}_{43} = \Omega_s^* \frac{-i(\rho_{33} - \rho_{44}) + \frac{\Omega_p^*}{\gamma_3 - 2i\delta_{ps}}\bar{\rho}_{41}}{\Gamma_{43} + 2i\delta_s + \frac{|\Omega_c|^2}{\gamma_3 + \gamma_2 + 2i\delta_{sc}}} \quad (3)$$

*hmalotai@ucalgary.ca

the optical response for the signal field and $\Gamma_{kl} = \gamma_k + \gamma_l$. We substitute Eq. (3) into Eq. (2) to obtain

$$\bar{\rho}_{14} = i\Omega_p \frac{(\rho_{11}-\rho_{44})\left(\Gamma_{43}+2i\delta_s+\frac{|\Omega_c|^2}{\Gamma_{32}+2i\delta_{sc}}\right)+(\rho_{11}-\rho_{44})\frac{|\Omega_p|^2}{\gamma_3-2i\delta_{ps}}+(\rho_{44}-\rho_{33})\frac{|\Omega_s|^2}{\gamma_3-2i\delta_{ps}}}{\left(\Gamma_{43}+2i\delta_s+\frac{|\Omega_c|^2}{\Gamma_{32}+2i\delta_{sc}}\right)\left(\gamma_4-2i\delta_p+\frac{|\Omega_c|^2}{\gamma_2-2i\delta_{pc}}+\frac{|\Omega_s|^2}{\gamma_3-2i\delta_{ps}}\right)+\frac{|\Omega_p|^2}{\gamma_3-2i\delta_{ps}}\left(\gamma_4-2i\delta_p+\frac{|\Omega_c|^2}{\gamma_2-2i\delta_{pc}}\right)}. \quad (4)$$

For an atomic gas in three dimensions with $\mathcal{N}$ the atomic density and $\boldsymbol{d}_{14}$ the dipole moment, the linear optical susceptibility is [3]

$$\chi_p = \frac{\mathcal{N}|\boldsymbol{d}_{14}|^2}{\epsilon_0}\frac{\bar{\rho}_{14}}{\Omega_p}. \quad (5)$$

Our Eq. (4) generalizes the previous expression for the response function [3], which focuses on the special case of equal detuning between all fields and ignores signal-field and nonlinear probe-field terms.

We calculate and plot $\mathrm{Im}[\chi_p]$ (absorption) in Fig. 2. In order to explain the parameter choices in Fig. 2, we refer to Fig. 1(a). Specifically, we consider ^{87}Rb and assign $|1\rangle$, $|2\rangle$, and $|3\rangle$ to the $5S_{1/2}$ level with $F = 1$, $m_F = 0$ and $F = 2$, $m_F = \{-2,0\}$, respectively. Level $|4\rangle$ corresponds to the $5P_{1/2}$ level with $F = 2$ and $m_F = -1$. The decay rates [7] and field strengths are given in the Fig. 2 caption for atomic density $10^{14}\mathrm{cm}^{-3}$.

Figure 2 exemplifies the features inherent in Eq. (4). First consider the case that $\Omega_s \equiv 0$, which decouples $|3\rangle$ from the dynamics and restores ordinary Λ-atom EIT. The semiclassical dressed picture of Fig. 1(b) clarifies the dynamics where we introduce two dressed states $|\pm\rangle$. The $\Omega_s \equiv 0$ line in Fig. 2 shows two EIT absorption peaks at $\delta_p^{\pm}$ corresponding to $|1\rangle \leftrightarrow |\pm\rangle$ transitions, respectively.

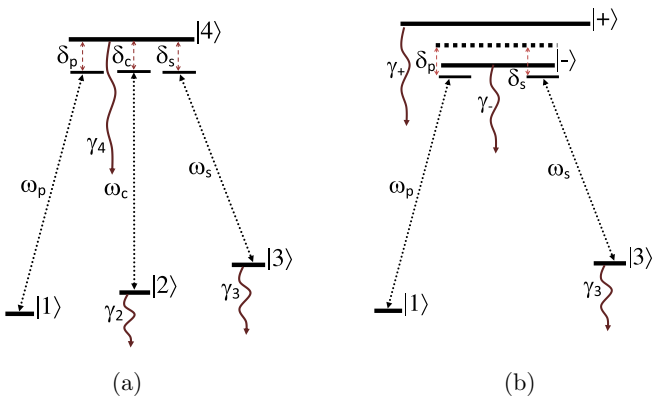

FIG. 1. (Color online) (a) Four-level tripod electronic structure with high-energy state $|4\rangle$ and lower-energy levels $|1\rangle$, $|2\rangle$, and $|3\rangle$ in order of increasing energy. Transitions are driven by probe (p), coupling (c), and signal (s) fields with frequencies ω_x and detunings δ_x with x$\in \{p,c,s\}$. Decay rates for level $|i\rangle$ are γ_i for $i \in \{2,3,4\}$. (b) Same atom in the semiclassical dressed state picture for strong c field, which corresponds to a double-Λ level structure. Levels $|2\rangle$ and $|4\rangle$ are hybridized into $|\pm\rangle$.

Mathematically, the semiclassical dressed picture is obtained by the unitary transformation [8,16]

$$\rho \mapsto U\rho U^\dagger, \quad U = \begin{pmatrix} 1 & 0 & 0 & 0 \\ 0 & \vartheta & 0 & \vartheta\varsigma \\ 0 & 0 & 1 & 0 \\ 0 & -\vartheta\varsigma^* & 0 & \vartheta \end{pmatrix}, \quad (6)$$

with $\varsigma := \frac{\sqrt{|\Omega_c|^2+\delta_c^2}+\delta_c}{\Omega_c}$ and $\vartheta := \frac{1}{\sqrt{1+|\varsigma|^2}}$. In this semiclassical dressed basis

$$\bar{\rho}_{1-} = \left(\vartheta\varsigma + \frac{i\vartheta\Omega_c^*}{\gamma_2 - 2i\delta_{pc}}\right)\bar{\rho}_{14} \quad (7)$$

and

$$\bar{\rho}_{1+} = \left(\vartheta - \frac{i\vartheta\varsigma^*\Omega_c^*}{\gamma_2 - 2i\delta_{pc}}\right)\bar{\rho}_{14}, \quad (8)$$

which are plotted in Fig. 3. Equations (7) and (8) are useful because the undressed state $\bar{\rho}_{14}$ corresponds to interfering transitions to $\bar{\rho}_{1\pm}$.

For $\Omega_s \neq 0$, we see in Fig. 2 that the second absorption peak at δ_p^+ is split by a transparency window with negative absorption, i.e., gain. This splitting of the second peak is due to the formation of a double-Λ electronic structure [9] shown in Fig. 1(b). Specifically, level $|+\rangle$ gives the absorption peak at δ_p^-, but the peak at δ_p^+ is split by competing transitions $|1\rangle \leftrightarrow |-\rangle$ and $|3\rangle \leftrightarrow |-\rangle$.

This explanation of competing transitions elucidates the splitting of the δ_p^+ peak but not the presence of gain in the second EIT window ($\delta_p = \delta_s$). In Fig. 3 gain in $\bar{\rho}_{1+}$ is evident over a wide domain of δ_p but cancels everywhere in the sum $\bar{\rho}_{1+} + \bar{\rho}_{1-}$ except in the narrow second EIT window. This gain is due to off-resonant driving to one of the upper levels. Both $\mathrm{Im}\bar{\rho}_{1\pm}$

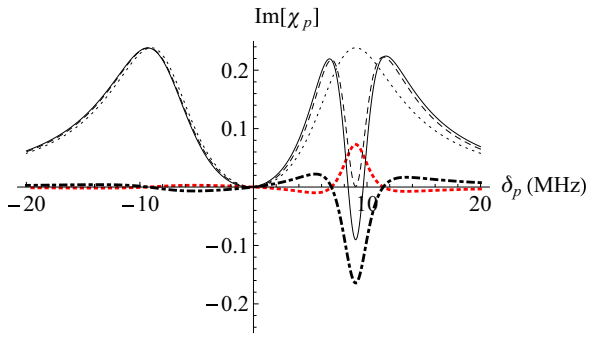

FIG. 2. (Color online) Absorption $\mathrm{Im}[\chi_p]$ vs probe detuning δ_p for $\gamma_4 = 18$ MHz, $\gamma_3 = 10$ kHz, $\gamma_2 = 40$ kHz, $\Omega_c = \gamma_4$, $\Omega_s = 0.3\gamma_4$, $\Omega_p = 0.2\gamma_4$, $\delta_s = 9$ MHz, and $\delta_c = 0$ with all terms of Eq. (4) included (solid line), with $\rho_{43} \equiv 0$ imposed (dashed line), the gain term (dot-dashed line), the nonlinear absorption term (dotted red line), and the case that $\Omega_s \equiv 0$ (dotted line).

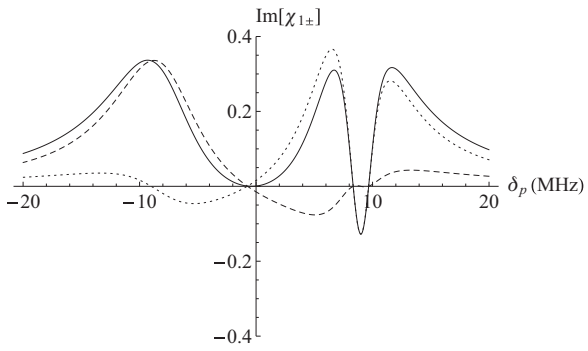

FIG. 3. Plot of $\mathrm{Im}(\chi_{1\pm})$ vs probe detuning δ_p for the same parameters as in Fig. 2 with $\bar{\rho}_{1+}$ (dashed line), $\bar{\rho}_{1-}$ (dotted line), and $\bar{\rho}_{1+} + \bar{\rho}_{1-}$ (solid line).

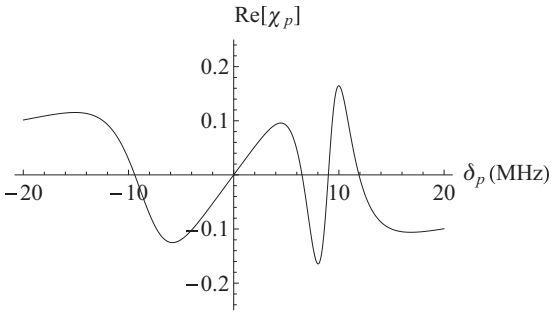

FIG. 4. Plot of $\mathrm{Re}[\chi_p]$ vs probe detuning δ_p for the same parameters as in Fig. 2.

contribute to the probe susceptibility, which is proportional to $\bar{\rho}_{14}$. The gain for the $|1\rangle \leftrightarrow |+\rangle$ is overwhelmed by the loss due to driving the $|1\rangle \leftrightarrow |-\rangle$ transition on or near resonance. This loss overwhelms the gain leading to no gain for the probe transition except in a narrow window as seen in Fig. 3.

As this gain is initially surprising, we investigate further using the undressed picture of Fig. 1(a). In the undressed picture the population in $|2\rangle$ and $|4\rangle$ vanishes at steady state because there is no decay from $|3\rangle$ to $|2\rangle$, i.e., $\gamma_{32} = 0$. Any population pumped by the coupling field to $|4\rangle$ will then decay to $|1\rangle$ and $|3\rangle$. At steady state, the population will be distributed between states $|1\rangle$ and $|3\rangle$. Thus, gain is not due to population inversion in $|4\rangle$ or due to hidden population inversion in $|\pm\rangle$ but rather due to quantum coherence inherent in $\bar{\rho}_{43}$, which is due to signal-field driving.

Mathematically, gain due to signal-driven coherence is evident in Eq. (2), which is a sum of two terms: one proportional to population difference $\rho_{11} - \rho_{44}$ and the other proportional $\bar{\rho}_{43}$. Gain occurs at $\delta_p = \delta_s$ for which the imaginary part of the first term is positive and the imaginary part of the second term is negative. Probe gain arises due to signal-driven coherence via $|1\rangle \leftrightarrow |3\rangle$ coherence: $\dot{\rho}_{13} = (-\frac{1}{2}\gamma_3 + i\delta_{ps})\rho_{13} - \frac{i}{2}(-\rho_{14}\Omega_s^* + \rho_{43}\Omega_p)$, which shows that this coherence is responsible for coupling the signal- and probe-driven transitions. This $|1\rangle \leftrightarrow |3\rangle$ coherence is crucial to establish the requisite interfering channels in order to enable gain to outweigh the effects of absorption [17,18].

The amplification can be partially understood as a Raman gain by ignoring level $|2\rangle$ and considering just the Λ system corresponding to the three levels $|1\rangle$, $|3\rangle$, and $|4\rangle$. Under the two-photon resonance condition, the signal pumps and the probe behave as an anti-Stokes field [19–21]. However, EIT effects introduce new physics. Specifically, the following usual Raman-gain conditions are not required in our system: The pump does not need to be much stronger than the Stokes field, population inversion of the lower levels is not required, and detuning from the upper level can be small. Equations (4) and (9) show dependence on population differences $\rho_{11} - \rho_{44}$ and $\rho_{33} - \rho_{44}$, which reduces to the usual Raman population condition $\rho_{33} - \rho_{11}$ in the limit $|\Omega_s| = |\Omega_p|$.

Probe dispersion is shown in Fig. 4. Group velocity is constant in each of the two EIT windows. For detuning δ_p chosen at the center of each window, dispersion is zero so the ratio of group velocities for each EIT window is thus the inverse of the ratio of the slopes for each window. From the plot, the group velocity at the first window evidently exceeds the group velocity at the second window for the given parameters.

The optical response of the signal field is given by

$$\bar{\rho}_{34} = i\Omega_s \frac{(\rho_{33}-\rho_{44})\left(\gamma_4 + 2i\delta_p + \frac{|\Omega_c|^2}{\gamma_2+2i\delta_{sc}}\right) + (\rho_{33}-\rho_{44})\frac{|\Omega_s|^2}{\gamma_3+2i\delta_{ps}} + (\rho_{44}-\rho_{11})\frac{|\Omega_p|^2}{\gamma_3+2i\delta_{ps}}}{\left(\Gamma_{43} - 2i\delta_s + \frac{|\Omega_c|^2}{\Gamma_{32}-2i\delta_{sc}} + \frac{|\Omega_p|^2}{\gamma_3+2i\delta_{ps}}\right)\left(\gamma_4 + 2i\delta_p + \frac{|\Omega_c|^2}{\gamma_2+2i\delta_{pc}}\right) + \frac{|\Omega_s|^2}{\gamma_3+2i\delta_{ps}}\left(\Gamma_{43} - 2i\delta_s + \frac{|\Omega_c|^2}{\Gamma_{32}-2i\delta_{pc}}\right)}. \quad (9)$$

The corresponding absorption and dispersion curves for the signal field are plotted in Figs. 5(a) and 5(b), respectively.

Similar to the probe-field cases shown in Figs. 2 and 4, we observe two EIT windows in the signal-field absorption plot and gain in the second window. From Figs. 2 and 5 we see that the first probe and signal EIT windows are both centered at δ_c. The second EIT windows are centered at $\delta_p = \delta_s$, which differs from δ_c. Gain is present in each of the linear susceptibilities for the signal and probe second EIT windows. Simultaneous slowing of beams and matching their group velocities is advantageous for enhancing interbeam interactions, such as for cross-phase modulation.

Here we have two transparency windows for each of the signal and probe beams. Now we seek to match group velocities for each of the signal and probe fields for the first EIT window and also for the second EIT window. In other words, we wish to have DEIT for the signal and probe for the first EIT windows and also to have DEIT for the second EIT windows of each of the signal and probe. Through this DDEIT phenomenon, one could send bichromatic signal and probe fields through the medium with the lower-frequency chromatic component of the signal and probe fields traveling with one simultaneously matched group velocity and the upper-frequency chromatic component also traveling through

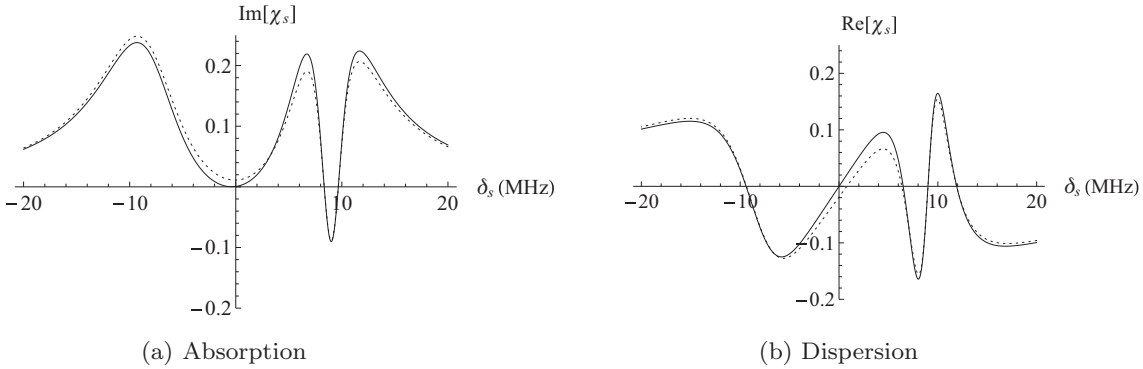

(a) Absorption (b) Dispersion

FIG. 5. (a) Absorption and (b) dispersion as a function of the signal detuning δ_s, analytical (solid line) and numerical (dotted line) solutions with $\Omega_s = 0.2\gamma_4$, $\Omega_p = 0.3\gamma_4$, $\delta_p = 9$ MHz and the other parameters as in Fig. 2.

the medium at a different but simultaneously matched group velocity

For group-velocity matching in ^{87}Rb with the same parameters as before, we choose field strengths $\Omega_s = 0.3\gamma_4 = \Omega_p$ and $\Omega_c = 1.0\gamma_4$. The resultant group velocities are nearly identical at 60.7 and 60.8 ms^{-1} for the probe and signal fields, respectively, in the first EIT window and 10.9 ms^{-1} for both the probe and signal field in the second EIT window. The two EIT windows for each signal and probe are separated by $\Omega_c/2 = 9.0$ MHz with a first-window full width at half maximum of 10.5 MHz and a second-window width of 2 MHz.

The second window is quite narrow but experimentally resolvable. This second EIT window for the probe has been observed for the ^{87}Rb D_1 line, although the width and other features of this window were not investigated [15]. Thus, simultaneous matching of signal and probe group velocities in each of the two EIT windows should be possible with reasonable experimental parameters.

Thus far we have assumed natural linewidths but now consider robustness subject to driving-field linewidth broadening and temperature-dependent Doppler broadening. Laser linewidth broadening dephases atomic transitions but does not modify atomic populations [22], hence is accounted for by a dephasing-rate replacement [15,23] $\gamma_\phi \to \gamma_\phi + \Delta$ in Eq. (1) with Δ the full width at half maximum of the laser line. Specifically, we modify the homogeneous dephasing rates by the laser-broadened dephasing rates for each of the probe, coupling, and signal fields and assume independence of all driving-field sources.

Doppler broadening is accounted for by averaging the complex susceptibility over a Maxwell distribution of velocities. For the D_1 line of ^{87}Rb, two-photon transitions are completely Doppler-free because the three driving fields drive approximately equal transition frequencies $\omega_p \approx \omega_c \approx \omega_s$. Therefore, each δ_{xy} in Eqs. (4) and (9) does not change under Doppler broadening. We compute the imaginary part of susceptibility using the same parameters as in Fig. 2 but for room temperature, i.e., 300 K, and show the result in Fig. 6. A comparison of these figures shows a reduction of EIT window width commensurate with past observations [24].

Furthermore, we observe a reduction in transparency and gain due to both the driving-field linewidth effect [23] and Doppler broadening [25]. Despite Doppler broadening, both windows are still evident and the second window is evidently more robust than the first with respect to Doppler broadening. The narrowness of the transparency window imposed by Doppler broadening could produce an ultraslow group velocity [26].

In summary, we have shown that a tripod Λ electronic energy structure in a four-level atom can yield rich phenomena, in particular double-double electromagnetically induced transparency with gain. We have used a semiclassical dressed picture to connect the Λ electronic structure to a double-Λ electronic structure to explain how each signal and probe field experience DEIT windows; this representation simplifies the master equation and engenders an intuitive understanding of Λ-atom coherent phenomena especially those that would otherwise appear as complicated dispersive phenomena. In the well studied case of DEIT, a signal and probe would each have an EIT window such that both fields can be slowed at the same time and also could interact via cross-phase modulation. In our case DDEIT exhibits DEIT for both the first EIT windows of the signal and probe and also for the second windows.

Our DDEIT scheme should be experimentally feasible and we have employed realistic parameters for ^{87}Rb including driving-laser linewidths and temperature [7,15]. Double EIT for the second EIT windows for the signal and probe fields do not just replicate the nature of the first because the second

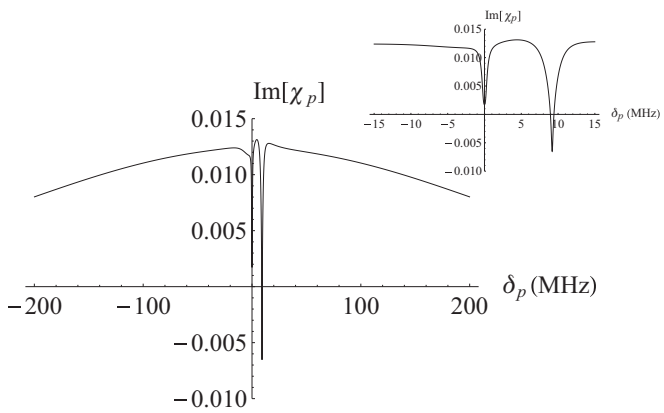

FIG. 6. Plot of Im[χ_p] as a function of probe detuning δ_p for the same parameters as in Fig. 2 with laser linewidths $\Delta_p = \Delta_c = \Delta_s = 0.1$ MHz and $T = 300$ K. The inset shows a magnified graph where EIT and gain are evident.

windows also show coherent gain and our scheme could be especially interesting for controlling bichromatic signal and probe fields.

We acknowledge valuable discussions with S. Rebic and P. Anisimov and support from AITF, CIFAR, PIMS, NSERC, and the China Thousand Talents Program.

[1] S. E. Harris, Phys. Today **50**(7), 36 (1997).
[2] A. I. Lvovsky, B. C. Sanders, and W. Tittel, Nat. Photon. **3**, 706 (2009).
[3] S. Rebić, D. Vitali, C. Ottaviani, P. Tombesi, M. Artoni, F. Cataliotti, and R. Corbalán, Phys. Rev. A **70**, 032317 (2004).
[4] A. Joshi and M. Xiao, Phys. Rev. A **72**, 062319 (2005).
[5] Z.-B. Wang, K.-P. Marzlin, and B. C. Sanders, Phys. Rev. Lett. **97**, 063901 (2006).
[6] C. Ottaviani, S. Rebić, D. Vitali, and P. Tombesi, Phys. Rev. A **73**, 010301 (2006).
[7] A. MacRae, G. Campbell, and A. I. Lvovsky, Opt. Lett. **33**, 2659 (2008).
[8] M. Fleischhauer, A. Imamoglu, and J. P. Marangos, Rev. Mod. Phys. **77**, 633 (2005).
[9] F. Vewinger, J. Appel, E. Figueroa, and A. I. Lvovsky, Opt. Lett. **32**, 2771 (2007).
[10] A. K. Patnaik, J. Q. Liang, and K. Hakuta, Phys. Rev. A **66**, 063808 (2002).
[11] V. Ahufinger, R. Corbalán, F. Cataliotti, S. Burger, F. Minardi, and C. Fort, Opt. Commun. **211**, 159 (2002).
[12] A. H. Safavi-Naeini, T. P. Mayer Alegre, J. Chan, M. Eichenfield, M. Winger, Q. Lin, J. T. Hill, D. E. Chang, and O. Painter, Nature (London) **472**, 69 (2011).
[13] A. A. Abdumalikov, Jr., O. Astafiev, A. M. Zagoskin, Y. A. Pashkin, Y. Nakamura, and J. S. Tsai, Phys. Rev. Lett. **104**, 193601 (2010).
[14] E. Paspalakis and P. L. Knight, Phys. Rev. A **66**, 015802 (2002).
[15] S. Li, X. Yang, X. Cao, C. Zhang, C. Xie, and H. Wang, J. Phys. B **40**, 3211 (2007).
[16] P. R. Berman, Phys. Rev. A **53**, 2627 (1996).
[17] O. Kocharovskaya, Phys. Rep. **219**, 175 (1992).
[18] J. L. Cohen and P. R. Berman, Phys. Rev. A **55**, 3900 (1997).
[19] Y. R. Shen and N. Bloembergen, Phys. Rev. **137**, A1787 (1965).
[20] N. Bloembergen and Y. R. Shen, Phys. Rev. **133**, A37 (1964).
[21] C. N. Alan and J. V. Moloney, *Nonlinear Optics* (Addison-Wesley, Redwood City, 1992).
[22] S. Sultana and M. S. Zubairy, Phys. Rev. A **49**, 438 (1994).
[23] B. Lü, W. H. Burkett, and M. Xiao, Phys. Rev. A **56**, 976 (1997).
[24] C. Y. Ye and A. S. Zibrov, Phys. Rev. A **65**, 023806 (2002).
[25] G. Vemuri and G. S. Agarwal, Phys. Rev. A **53**, 1060 (1996).
[26] M. M. Kash, V. A. Sautenkov, A. S. Zibrov, L. Hollberg, G. R. Welch, M. D. Lukin, Y. Rostovtsev, E. S. Fry, and M. O. Scully, Phys. Rev. Lett. **82**, 5229 (1999).